J Therm Spray Tech
https://doi.org/10.1007/s11666-024-01819-y

ORIGINAL RESEARCH ARTICLE

Effect of Powder Oxidation on Microstructures and Mechanical Properties of Cold-Sprayed Nickel Coatings and Improvement by Post-spray Heat Treatment

Zhengmao Zhang[1] · Wenya Li[1] · Jingwen Yang[1] · Yaxin Xu[1] · ChunJie Huang[1]

Submitted: 29 April 2024 / in revised form: 3 July 2024 / Accepted: 9 July 2024

Abstract This study investigated the effect of powder pre-oxidation on the microstructures and mechanical properties of cold-sprayed nickel coatings. The artificially pre-oxidized nickel powders at 200, 300 and 400 °C for 5 h show the resulting oxygen contents of 0.27, 0.36 and 0.41 wt.%, as compared to 0.21 wt.% in the feedstock powder. Microstructurally, the higher oxygen contents of the impact particles significantly increased in both the number and size of the pores in the as-sprayed coatings by using the pe-oxidized powders, as a result of the porosities of 0.7, 1.5 and 3.3% compared to 0.4% by using the as-atomized powder (natural oxidation condition). Mechanically, the increased oxygen contents of powders result in the reduced properties for the as-sprayed Ni coatings, as the microhardness of 263.2 $HV_{0.1}$, 245.3 $HV_{0.1}$ and 236.3 $HV_{0.1}$ and the tensile strength of 94, 76 and 61 MPa by using oxidized powders compared to those of 289.2 $HV_{0.1}$ and 208 MPa by using natural oxidation powder. In addition, post-spray heat treatment at 800 °C for 2 h effectively reduces the small-sized pores and nonbonded particle-particle boundaries within the coatings, which is attributed to a combination effect of annealing twins and dislocation slip during heat treatment. As a result, the microhardness significantly decreased to 135.3 $HV_{0.1}$, 126.7 $HV_{0.1}$, 124.5 $HV_{0.1}$ and 114.7 $HV_{0.1}$, while the tensile strength is increased to 210, 166, 133 and 117 MPa, respectively.

Keywords cold spray · mechanical property · microstructure · nickel (Ni) · oxygen content · post-spray heat treatment

Introduction

Cold spray (CS) is a process in which micron-sized metal powder particles impact a substrate at high speeds under specific conditions, resulting in severe plastic deformation and deposit bonding with the substrate (Ref 1-6). Compared to the conventional thermal spray methods to fabricate metal coatings (Ref 7-9), CS is characterized by the low-temperature, high-velocity deposition of solid particles. In addition, the residual stresses generated in the CS process are small and compressive, facilitating a thick deposit. Therefore, CS is an effective method for preparing highly pure and oxidation-free Ni coatings (Ref 10-13).

Ni is widely used in various industrial fields due to its excellent corrosion resistance. The current commonly used Ni coating preparation technology is electroplating, but it causes serious pollution. Therefore, adopting a more environmentally friendly CS process to prepare Ni coatings is even more crucial. To promote the widespread use of cold-sprayed Ni coatings, their properties must be effectively tuned, especially regarding crucial mechanical property indicators such as strength and plasticity. Previous studies (Ref 14-20) have shown that the oxide films on the surfaces of high-speed metal particles need to be crushed and extruded during the CS process to enable metallurgical bonding of exposed fresh metal under high-impact pressure. For examples, Li et al. (Ref 21-23) found for the first

✉ Wenya Li
liwy@nwpu.edu.cn

ChunJie Huang
huangc@nwpu.edu.cn

[1] State Key Laboratory of Solidification Processing, Shaanxi Key Laboratory of Friction Welding Technologies, School of Materials Science and Engineering, Northwestern Polytechnical University, Xi'an 710072, China

Published online: 22 August 2024

time that the oxide film hindered the formation of metallurgical bonding between the particles and the substrate during the CS process and significantly increased the critical velocity of the impact particles. Furthermore, Rahmati et al. (Ref 24) verified the formation of metallurgical bonding between Cu particles and the substrate during the CS process, and the effect of the thickness of the oxide film on the metallurgical bonding was investigated using numerical simulation. Ichikawa et al. (Ref 25) experimentally demonstrated that oxide-free regions of deposited particles formed metallic bonds, resulting in a higher bonding strength between the particles and the substrate than the substrate. Meanwhile, the oxide film on the top of the particles remained in the coating, and the bonding strength was significantly lower than that of the substrate, significantly reducing the coating's mechanical properties.

In addition, the "shot peening effect" formed by the high-velocity impact of particles during the CS process leads to higher hardness of the coating, but the deposited particle interface is more mechanically bonded, resulting in high strength and poor plasticity of the coating. the non-bonded particle-particle boundaries within the coating cause stress concentrations that can be potential sources of cracks, leading to crack nucleation and growth (Ref 26). Besides using expensive helium as the working gas, optimizing process parameters to eliminate such defects in the cold-sprayed coatings is challenging. Therefore, an appropriate post-treatment method is needed to improve the structure and performance of cold-sprayed Ni coatings. It was suggested that recrystallization and recovery can significantly improve plasticity (Ref 27). Zou et al. (Ref 28) investigated the microstructural evolution of cold-sprayed and heat-treated states for Ni coatings by using EBSD analysis. The microstructural transition was homogenous, with the gradual disappearance of substructures within the grains, an increase in grain size and a complete release of residual stresses. By comparing the microhardness indentation patterns of cold-sprayed and heat-treated Ni coatings, it was found that the heat-treated Ni coatings showed significant improvement in plasticity and toughness with reduced hardness. Moreover, Koivuluoto et al. (Ref 29) developed a comparative analysis of the fracture surfaces of cold-sprayed and heat-treated Ni coatings and found that the tensile fracture behavior transitioned from brittle fracture to mixed brittle/ductile fracture and finally to ductile fracture.

This study aims to investigate the effect of oxygen contents in raw material powder on the microstructure and mechanical properties of cold-sprayed Ni coatings. Furthermore, heat treatment is proposed to enhance the mechanical properties and reveal the evolution of microstructure and mechanical properties of cold-sprayed Ni coatings, which will provide valuable insights for a wide range of applications of cold-sprayed Ni coatings.

Materials and Methods

Nitrogen-atomized Ni powder (TIJO, China) with a purity of $> 99.5\%$ was used as powder feedstock. The natural oxidation (named NO) was processed under powder storage (> 6 months) at ambient temperature in the original air packing atmosphere. The NO powder was observed to exhibit an irregular morphology (Fig. 1a) by scanning electron microscopy (SEM, VEGA 3 LMU, TESCAN, Czech) and the range of particle size distribution with an average powder size D50 of 45 μm (Ref 11). To obtain different oxygen contents of the original feedstock, the powder was artificially oxidized in a muffle furnace (SX2-12TP, XINKYO, China) for 5 h at 200, 300 and 400 °C and then cooled by the furnace, named as AO_1, AO_2 and AO_3, respectively. The oxygen contents of the four types of feedstocks measured by an oxygen–nitrogen–hydrogen analyzer (ONH836, HMC, USA) were 0.21, 0.27, 0.36 and 0.41%, respectively, as shown in Fig. 1(b).

A commercial high-pressure cold spray system developed by Northwestern Polytechnical University, China, was applied. The spraying experiment for the full coatings was performed using nitrogen as the working gas with a gas pressure of about 3.8 MPa and a gas temperature of about 600 °C. The spraying distance and the nozzle transverse speed were set to 20 mm and 20 mm/s, respectively. The pure Ni plates, as the substrate material, underwent sandblasting prior to spraying. This process eliminated oxide layers and impurities, revealing a fresh metal surface that facilitated strong bonding between the substrate and powder.

The heat treatment tests were carried out using a vacuum heat treatment furnace (SK2-TPA2, XINKYO, China) with the inert gas argon as a protective gas, and the vacuum level used during the heat treatment was 1×10^{-3}. The selected heat treatment temperature was 800 °C with a holding time of 2 h, followed by slowly cooling down with the furnace to room temperature. The heat-treated coatings were designated HT-NO, HT-AO_1, HT-AO_2 and HT-AO_3.

The cross sections of coatings were analyzed with an optical microscope (VHX-5000, KEYENCE, Japan), and the porosity was measured by the Image Pro Plus software. The etchant used for the Ni coatings was formulated by mixing 40% HNO_3 and 60% CH_3COOH. The microstructural details were analyzed by electron backscatter diffraction (EBSD, Gemini 300, ZEISS, Germany). The EBSD data were evaluated at 15 KV in a step size of 0.2 μm and then processed to image quality (IQ), grain orientation spread (GOS), grain boundaries (GBs), inverse

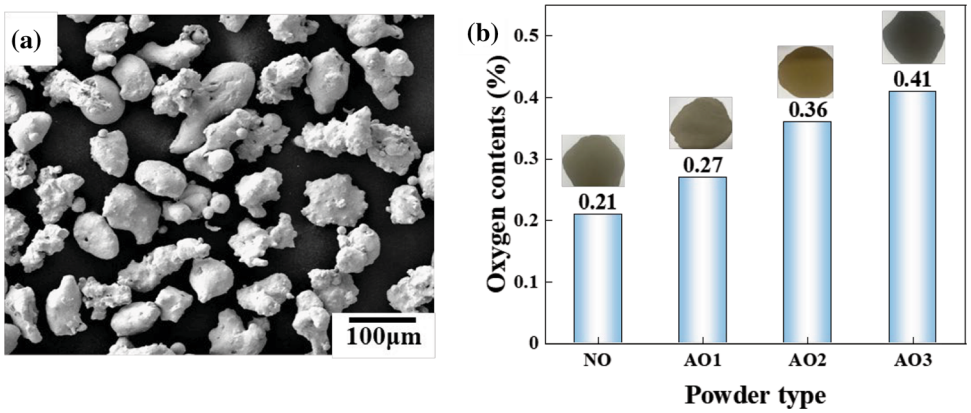

Fig. 1 (a) Ni powder morphologies observed by SEM (Ref 11); (b) oxygen contents under different oxidation conditions. Effect of Powder Particle Size on Microstructure and Mechanical Properties of Cold-Sprayed Pure Nickel Coatings, Z.M. Zhang, Y.X. Xu, W.Y. Li, J.W. Yang, C.J. Huang, Journal of Thermal Spray Technology, Volume 33, Springer Nature, 2024, reproduced with permission from SNCSC

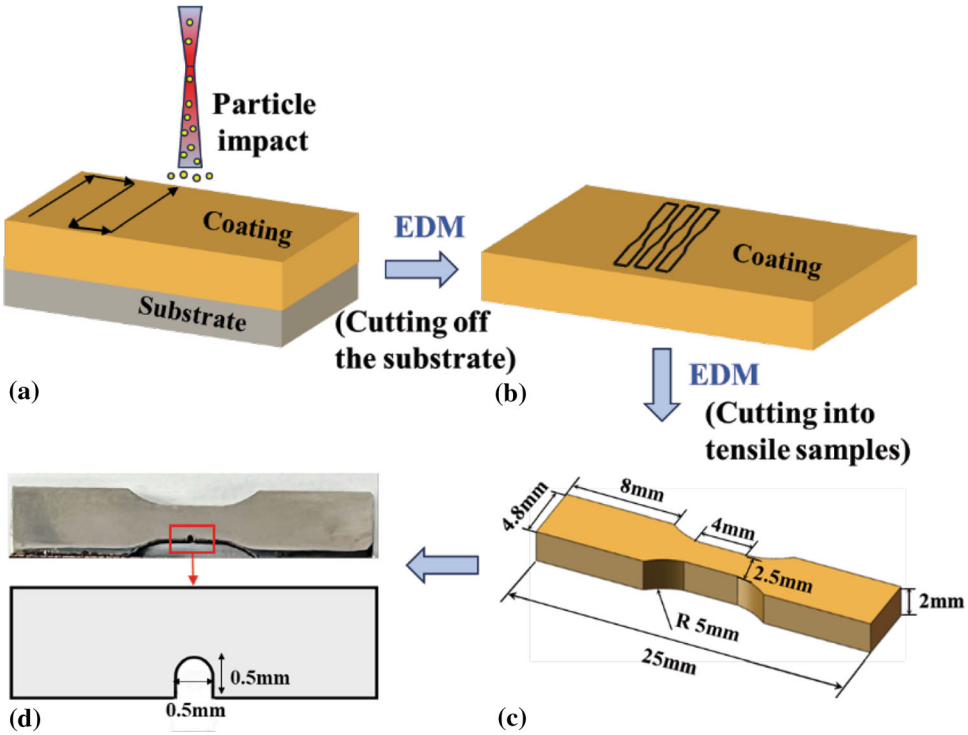

Fig. 2 The schematic diagram of the position and dimensions of a tensile sample. (a) spray direction; (b) the sampling location; (c) the size of a tensile sample; (d) a photographic image of an in-situ tensile sample

pole figure (IPF) and kernel average misorientation (KAM) maps by AZtec software. Microhardness was determined on the polished cross sections as $HV_{0.1}$ under a load of 100 g and a holding time of 15 s (AMH43, LECO, USA). The tensile tests were performed by an electronic universal mechanical testing machine (3382, INSTRON, USA) with a tensile speed of 0.12 mm/s. The geometry and dimensions of the tensile sample are shown in Fig. 2(a), (b) and (c). The in situ tensile tests were performed by an in situ dynamic mechanics experimental system (IBTC-5000 CARE, China) with a tensile speed of 10N/s. All the tensile tests use three samples and take the average value as the test result. The schematic diagram of the in situ tensile machine and a tensile sample, as shown in Fig. 2(d). The purpose of prefabricated notches during the in situ tensile test is to ensure that the specimen can start to fracture along this place and facilitate to capture crack propagation behavior under OM. Digital image correlation (DIC) was

used to acquire information about coatings' local stress and deformation. In the current work, the evolution of the strain field in Ni coatings during in situ tensile was captured at a frame rate of 160 fps using a measurement system (XTDIC-Micro-SD, XTOP, China).

Results and Discussions

Microstructures of As-Sprayed Coatings

Figure 3(a), (b), (c) and (d) shows the cross-sectional microstructures of Ni coatings using NO, AO_1, AO_2 and

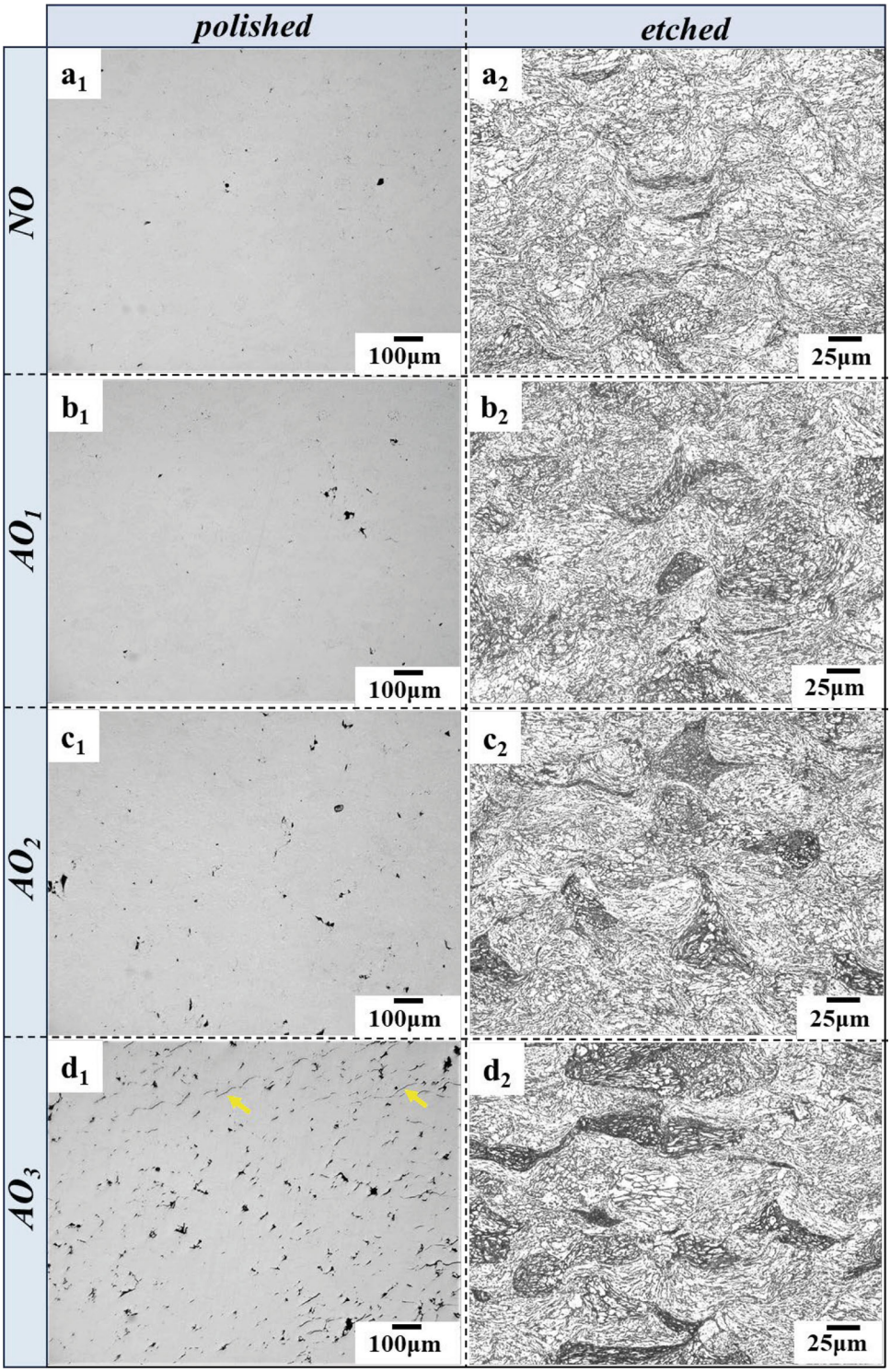

Fig. 3 OM cross-sectional morphologies of as-sprayed Ni coatings produced by different oxidation conditions: (a_1-a_2) NO (Ref 11), (b_1-b_2) AO_1, (c_1-c_2) AO_2, (d_1-d_2) AO_3; (a_1-d_1) polished microstructures at low magnification, (a_2-d_2) etched microstructures at high magnification. The yellow arrows represent the weakly bounding interface between particles. Effect of Powder Particle Size on Microstructure and Mechanical Properties of Cold-Sprayed Pure Nickel Coatings, Z.M. Zhang, Y.X. Xu, W.Y. Li, J.W. Yang, C.J. Huang, Journal of Thermal Spray Technology, Volume 33, Springer Nature, 2024, reproduced with permission from SNCSC

AO_3 as feedstock powders. Within the examined parameter ranges, the coatings have a high density and a low number of pores when the oxygen contents are at 0.21 (NO) and 0.27 wt.% (AO_1). However, the number and size of pore defects in the coatings increase significantly with increasing oxygen contents of the feedstock powders. Moreover, for the coating using AO_3 as feedstock powder (Fig. 3d_1-d_2), many weakly bonded and nonbonded interfaces between particles appear in the coating. From the OM images of Ni coatings, the porosity of Ni coatings using NO, AO_1, AO_2 and AO_3 as feedstock powders is 0.4, 0.7, 1.5 and 3.3, respectively. The defect characteristics, including defect size, content and distribution, are crucial factors that influence the quality of coatings. Quantifying the number and size of defects in Ni coatings can facilitate further investigation of the influence of defect characteristics on the mechanical properties of Ni coatings.

An increase in the oxygen content of feedstock powder leads to an increase in the thickness of the oxide film on the surface. A previous study by Li et al. (Ref 21) has demonstrated that as the oxide film of the particle surface becomes thicker, the impacting particles require higher kinetic energy to rupture and extrude the oxide film upon reaching the substrate, thus leading to a notable increase in the critical velocity of powder particles. Moreover, under the same spraying parameters conditions, the increase in oxygen content complicates the effective removal of the oxide film during particle–particle bonding, and the remaining oxide film elevates the proportion of weakly bound or unbound interfaces between particles in the coating, thus reducing the overall density of the coating.

EBSD can provide valuable information for understanding the interfacial characteristics of Ni coatings, particularly in revealing grain shapes and sizes, and deformation pattern structures (Ref 30). Moreover, a detailed investigation of the cold-sprayed Ni particles is beneficial in further revealing the effect of oxygen content on the microstructure of Ni coatings. Figure 4 shows the EBSD data for the cross-sectional regions of Ni coatings with different oxygen-content powders. By analyzing the IPF (Fig. 4a_1-d_1) maps, it is evident that Ni particles have undergone significant changes in grain shapes and sizes at the boundaries, which suggests the influence of severe plastic deformation during particle deposition. The dynamic recrystallization leads to a pronounced refinement of grains at the interfaces, thus producing a large number of refined grains (Ref 31). Meanwhile, the deformation of the particle inners is little, resulting in grain sizes significantly larger than those observed at particle-particle boundaries.

As the oxygen content in the feedstock powder increases, removing the adhered thick oxide films on the particle surfaces is difficult, leading to a little reduction in the degree of plastic deformation within the deposited particles (Ref 14). As a result, a large number of low-angle grain boundaries are observed, as illustrated in Fig. 4(a_2-d_2). The KAM maps (Fig. 4a_3-d_3) indicate that the dislocation density at the boundaries of the deformed particles is significantly lower than that in the interiors, which is attributed to the adsorption effect of the dislocations by the large-angle grain boundaries. However, an increase in the oxygen content of the feedstock powder leads to an overall decrease in the dislocation density of the coatings. This decrease can be attributed to the fact that some of the internal stresses are released from the feedstock powder during the heating of the pre-oxidation process, which results in a lower dislocation density within the grains.

Mechanical Properties of As-Sprayed Coatings

Microhardness

Figure 5 illustrates the microhardness of Ni coatings using NO, AO_1, AO_2 and AO_3 as feedstock powders, and the corresponding microhardness is 289.2, 263.2, 245.4 and 236.3 $HV_{0.1}$, respectively. Previous research (Ref 11) has demonstrated that deposit microhardness is closely related to the presence and distribution of internal defects. As the oxygen content of the used feedstock powders increases, the plastic deformation of impact particles decreases, and the work-hardening effect diminishes. The increase in oxygen content not only leads to the formation of large-sized pore defects but also promotes the occurrence of nonbonded interfaces within the coatings. Consequently, the density of the coatings decreases (see Fig. 3), adversely affecting the coating microhardness.

Tensile Properties

Figure 6 depicts the stress versus strain curves of Ni coatings using NO, AO_1, AO_2 and AO_3 as feedstock powders, and the tensile strengths are 208, 94, 76 and 61 MPa, respectively. The comparison shows that the tensile strength of the coatings significantly decreases when the powder used is pre-oxidized at 200 °C for 5 h compared to NO powder. In addition, the tensile strength decreases further with increasing oxygen content. This suggests that artificially oxidized feedstock powders significantly increase the oxide film thickness on the particle surface. As a result, the presence of a large number of nonbonded interfaces between the deformed particles due to the inclusion of oxide film significantly reduced the tensile strength of the obtained coatings.

Figure 7 presents the tensile fracture morphology of Ni coatings under varying powder oxygen content conditions. The cold-sprayed Ni coatings under different oxygen containing powder conditions failed to exhibit a yield stage

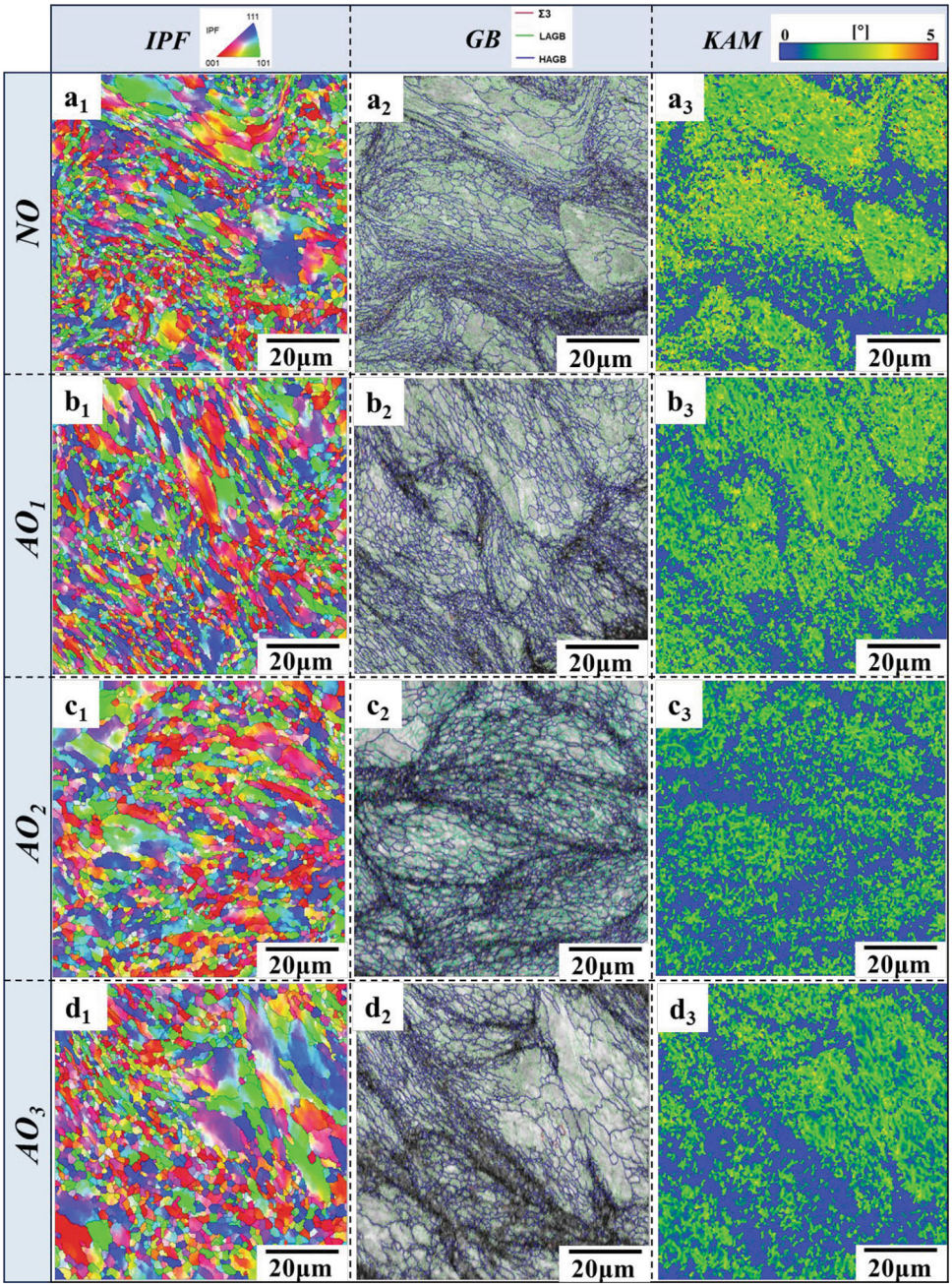

Fig. 4 EBSD data of as-sprayed Ni coatings with different oxygen-content powders: (a_1-d_1) IPF maps, (a_2-d_2) GB maps, and (a_3-d_3) KAM maps. (a_1-a_3) NO powder (Ref 11), (b_1-b_3) AO_1 powder, (c_1-c_3) AO_2 powder, and (d_1-d_3) AO_3 powder. Effect of Powder Particle Size on Microstructure and Mechanical Properties of Cold-Sprayed Pure Nickel Coatings, Z.M. Zhang, Y.X. Xu, W.Y. Li, J.W. Yang, C.J. Huang, Journal of Thermal Spray Technology, Volume 33, Springer Nature, 2024, reproduced with permission from SNCSC

during the tensile process, resulting in brittle fracture characteristics. For the coating with the feedstock of NO powder (Fig. 7a_1-a_2), some tear lines appear inside the particles, indicating that the strength of coating comes from mechanical and metallurgical bonding between the particles. As the oxygen content of the powder further increases, there is a transition from a combination from metallurgical and mechanical to only mechanical as the powder oxidizes. The particle boundaries are visible and relatively smooth, with numerous narrow and elongated pores at the particle interfaces, as shown the yellow arrows in Fig. 7(c_2). These pores serve as weak areas when the coating is subjected to external forces, leading to crack propagation along the particle interfaces and eventual brittle fracture.

Figure 8 shows the OM images of Ni coatings using NO and AO_1 as feedstock powders before and after crack initiation during in-situ tensile testing. It can be seen that the cracks initiate at the prefabricated notch and propagate along the weak areas such as particle-particle boundaries and pores when the coating is subjected to tensile stress, eventually leading to fracture, as shown in the red box in Fig. 8(b_1-b_2). To investigate the role of artificial oxidation and possible crack growth mechanisms in direct correlation

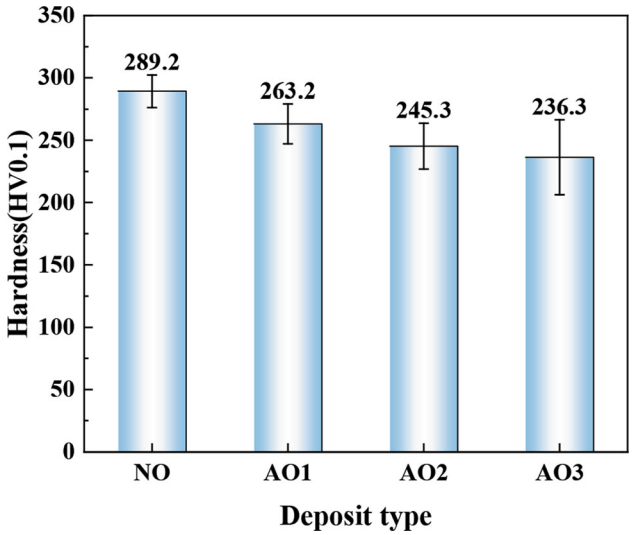

Fig. 5 Microhardness of as-sprayed Ni coatings by using different oxidized powders

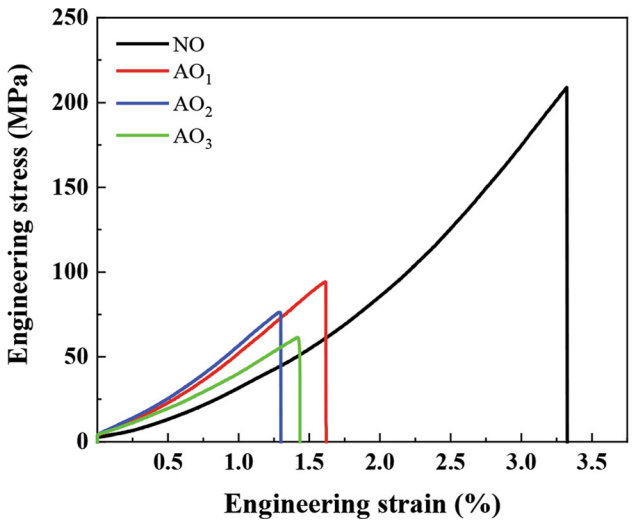

Fig. 6 Tensile stress vs. strain curves of as-sprayed Ni coatings produced with different oxidized powders

to the deformed microstructures of the as-sprayed Ni coatings, DIC was used to analyze the local deformation behavior for NO and AO_1 coatings, as presented in Fig. 8(c_1-c_2). It is evident that the maximum strain occurs at the pre-notch during in situ tensile testing. In addition, there is a notable stress concentration in the direction of crack propagation, thus resulting in a local true strain significantly higher than in other areas. Due to the limitation of the frame rate of OM, only one image can be captured every 10N during the in-situ tensile. As the strength of the Ni coating decreases, the time interval between crack initiation and crack propagation shortens. Therefore, for the coatings using AO_2 and AO_3 as feedstock powders, it is difficult to capture the crack initiation during the in situ tensile process, as shown in Fig. 9.

Microstructures of Post-spray Heat-Treated Coatings

During the cold spray process, significant work hardening occurs due to the extensive plastic deformation of deposited particles, resulting in the as-sprayed coating exhibiting characteristics such as high strength, hardness and low plasticity. Furthermore, the differing strains and strain rates between the interface and center of deformed particles result in an uneven microstructure in deposited particles. This non-uniform microstructure accumulates residual stress at the particle bonding interface, diminishing its mechanical properties. The inherent defects of as-sprayed coatings are challenging to eliminate through cold spray parameter optimization. Consequently, heat treatment is essential to enhance the microstructure and properties of as-sprayed Ni coatings.

Figure 10 exhibits the OM morphology of Ni coatings with different oxygen contents by heat treatment temperature of 800 °C for 2 h. Regarding the HT-NO coating, it exhibits a minimal presence of pores and weak bonding interfaces. Conversely, in the case of HT-AO_1 and HT-AO_2 coatings, as the oxygen content of the powder increases, the unbonded interfaces also increase within the heat-treated coating. This phenomenon mirrors the corresponding characteristics observed in the as-sprayed coatings. As for the HT-AO_3 coating, despite the application of heat treatment, the elimination of sizable pores within the as-sprayed coating remains challenging. Consequently, these large pores persist even after the heat treatment process. This suggests that improved atomic diffusion between particle interfaces has accelerated the migration of various defects (such as unbound interfaces and pores) toward grain boundaries and particle interfaces, resulting in the disappearance of small pore clusters. Furthermore, the etched morphology of Ni coatings under different oxygen content after heat treatment is illustrated in Fig. 10(a_2-d_2). Significant recrystallization and partial grain growth are observed within heat-treated Ni coatings, as opposed to numerous elongated grains at the particle interface in as-sprayed coatings. The growth of grains at some particle interfaces indicates substantial local diffusion and metallurgical bonding, resulting in a more uniform grain size distribution.

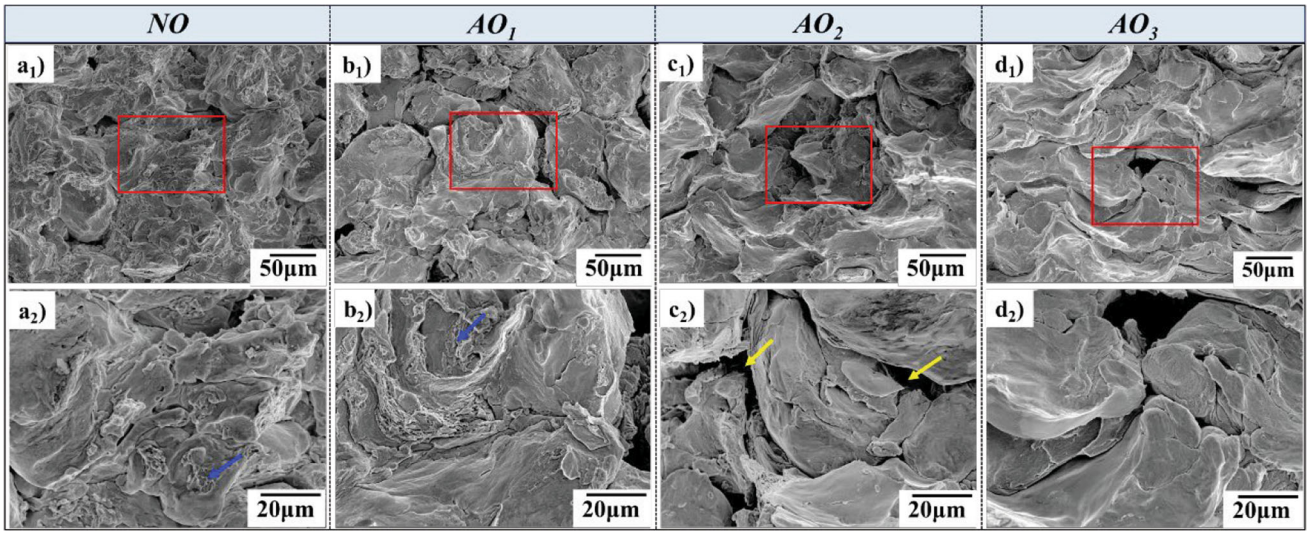

Fig. 7 SEM fractographic images of as-sprayed Ni coatings produced with different oxidized powders: (a_1-a_2) NO (Ref 11), (b_1-b_2) AO_1, (c_1-c_2) AO_2, and (d_1-d_2) AO_3. (a_2-d_2) respective enlarged views of the red boxes in (a_1-d_1). The blue arrows represent the tear lines inside the particles. The yellow arrows represent the unbounding interface between particles. Effect of Powder Particle Size on Microstructure and Mechanical Properties of Cold-Sprayed Pure Nickel Coatings, Z.M. Zhang, Y.X. Xu, W.Y. Li, J.W. Yang, C.J. Huang, Journal of Thermal Spray Technology, Volume 33, Springer Nature, 2024, reproduced with permission from SNCSC (Color figure online)

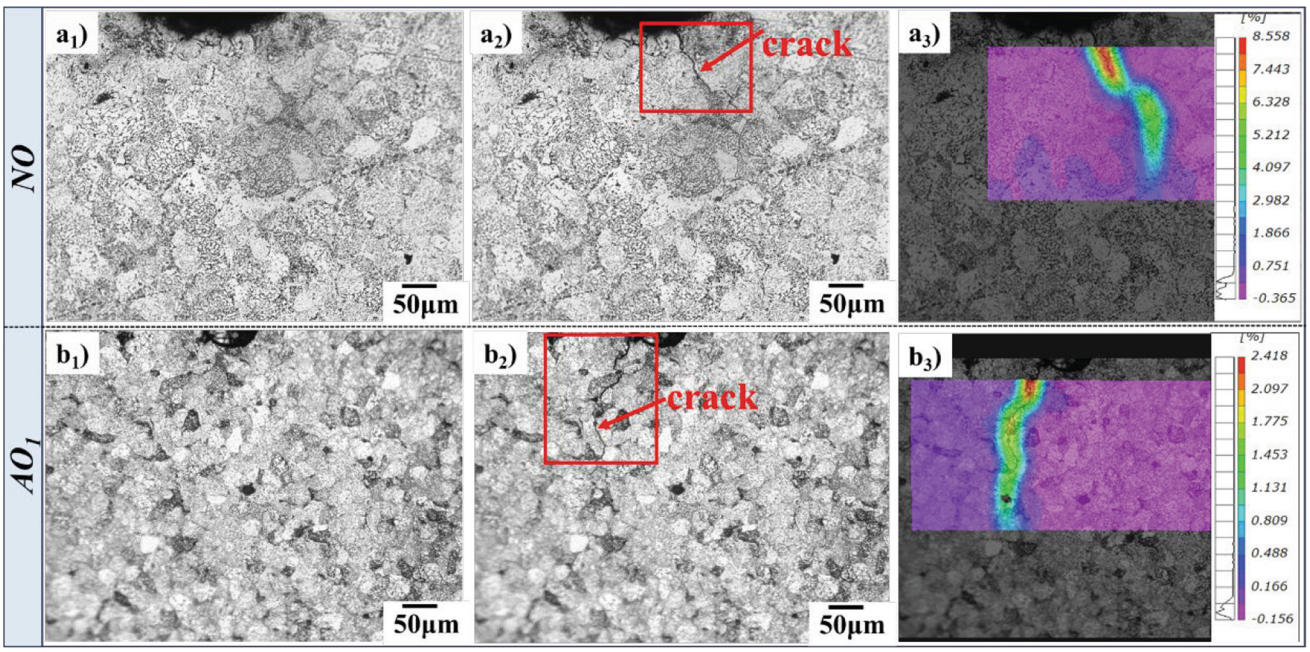

Fig. 8 OM images of Ni coatings before and after in-situ tensile with different oxygen-content powders: (a_1-a_3) NO, (b_1-b_3) AO_1, (a_1-b_1) before coating fracture; (a_2-b_2) after coating fracture, respectively. In the red box is the crack. (a_3-b_3) the evolution of the strain field (Color figure online)

During the cold spray process, the broken and extruded oxide film on the particle surface allows the fresh metal surface to form a good metallurgical bond, while the remaining unbroken oxide film in the coating forms weakly bound or unbound interfaces. The disappearance of particle interfaces is attributed to the combined effect of atomic diffusion and grain growth. However, during the heat treatment process, the thicker oxide film hinders the diffusion of some atoms at the particle interface, impeding interface healing. These unhealed interfaces become the

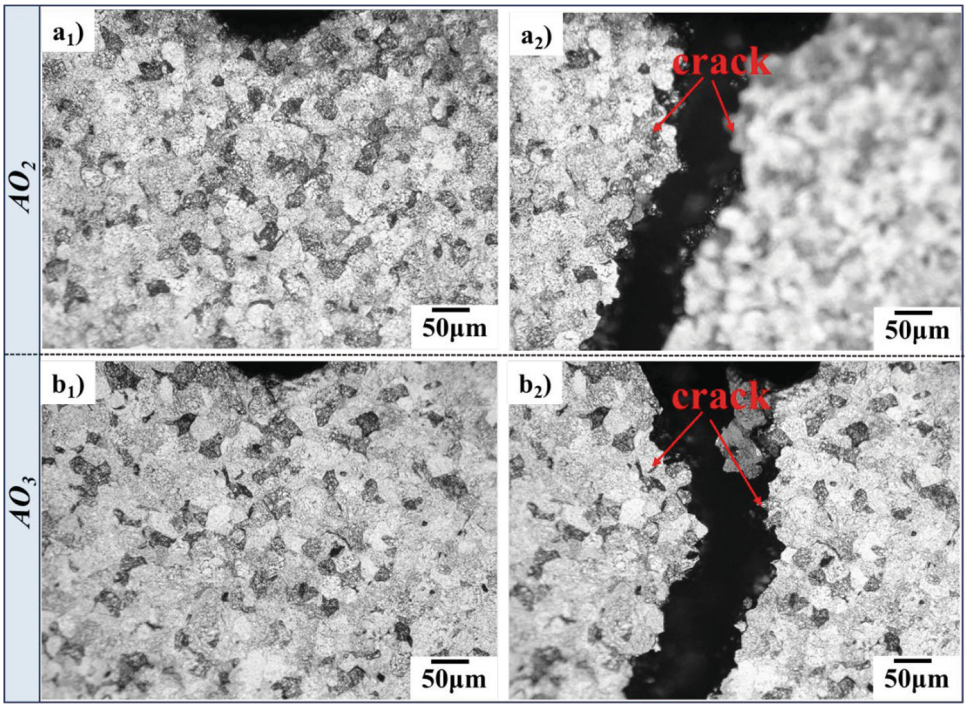

Fig. 9 OM images of Ni coatings before and after in-situ tensile with different powder oxygen content: (a_1-a_2) OA_2, (b_1-b_2) AO_3; (a_1-b_1) before coating fracture; (a_2-b_2) show the microstructures in the vicinity of the critical crack. The red arrows indicate the cracks (Color figure online)

source of cracks in the coating, negatively impacting its performance.

Detailed investigations of the internal interfaces of coating microstructures are needed to reveal the influence of heat treatment on the as-sprayed coatings. Figure 11 exhibits the EBSD data of the heat-treated coatings with different oxygen content. The IPF maps in Fig. 11(a_1-b_1) reveal that compared to the as-sprayed coatings, the internal grain shape of the heat-treated coatings changes from "flattened" deformed sub-grains to uniformly distributed equiaxed grains, with also an increase in grain size. The Ni particles undergo evident recovery and recrystallization processes at an annealing temperature of 800 °C, and the quantity of low-angle grain boundaries (LAGB) decreases, continuously replaced by high-angle grain boundaries (HAGBs) and Σ3 grain boundaries, as shown in Fig. 11(a_2-d_2). As indicated in the KAM map in Fig. 11(a_3-d_3), the dislocation density and stress concentration within the particles significantly decrease, corresponding to the reduction of LAGBs. Fig. 11(a_4-d_4) shows that deformed grains are replaced by recrystallized grains and sub-grains. The cooperative deformation effect of recrystallized grains and the hindrance effect of high-angle grain boundaries on dislocations can positively contribute to the strength and plasticity of the Ni coatings. With the increase in feedstock powder oxygen content, the proportion of recrystallized grains in the heat-treated coatings decreases, indicating a significant reduction in the degree of recrystallization of the coating. This is mainly due to the distribution of oxide film as finely dispersed inclusions at the particle interfaces and grain boundaries, which severely hinders the nucleation of sub-grains and the subsequent grain growth.

Mechanical Properties of Post-spray Heat-Treated Coatings

Microhardness

Figure 12 shows the average microhardness of the heat-treated coatings with different oxygen content. Compared to the as-sprayed coatings, the microhardness of the heat-treated coatings significantly decreases. The coating using AO_3 as feedstock powder exhibits the lowest average microhardness, measuring only 114.7 $HV_{0.1}$, which is close to the hardness of the Ni substrate (115.9 $HV_{0.1}$). The high microhardness of the as-sprayed coating is attributed to the shot peening effect during the cold spray process, where a large number of high-speed particles impact the substrate, leading to work hardening and an increase in microhardness of the deposited particles. After heat treatment, internal grain recovery and recrystallization occur within the as-sprayed coatings, resulting in continuous grain growth and large-angle grain boundaries that continually move. Consequently, the work-hardening effect caused by severe plastic deformation of the impacting particles diminishes, reducing dislocation density and eliminating

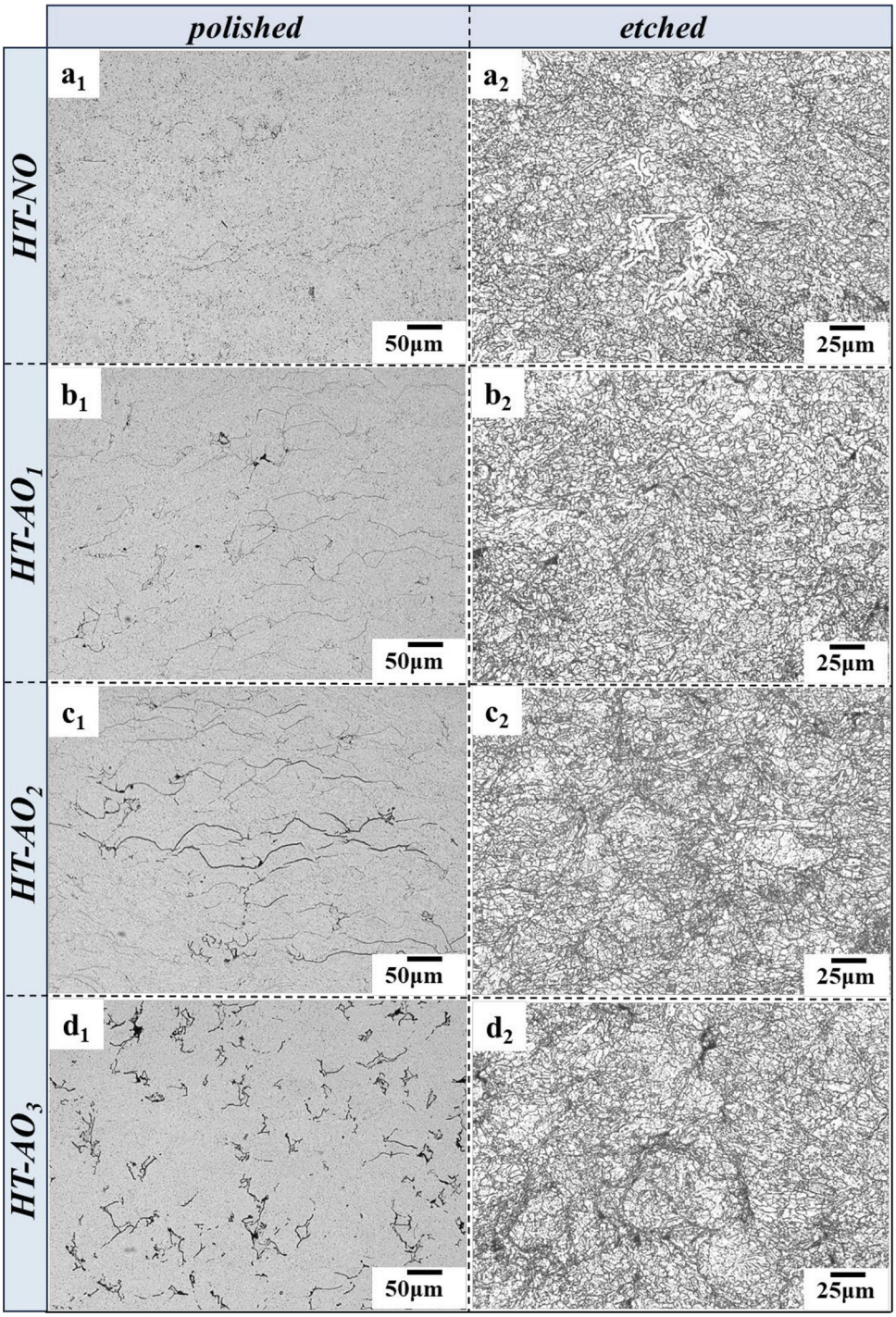

Fig. 10 OM cross-sectional morphologies of post-spray heat-treated Ni coatings produced with different oxidized powders: (a_1-a_2) HT-NO, (b_1-b_2) HT-AO_1, (c_1-c_2) HT-AO_2, and (d_1-d_2) HT-AO_3; (a_1-d_1) polished microstructures at low magnification, (a_2-d_2) etched microstructures at high magnification

internal stress, ultimately causing a rapid decrease in the microhardness of the heat-treated coatings.

Tensile Properties

Figure 13 depicts the tensile stress versus strain curves of the heat-treated Ni coatings with different oxygen content. Compared to the as-sprayed coatings, the strength and plasticity of the heat-treated coatings have been enhanced. For the coating using NO as feedstock powder, the tensile strength before and after heat treatment is 208 and 211 MPa, respectively. Although the strength of the coating shows a slight increase, the enhanced thermal diffusion increases the number of metallurgical bonding interfaces

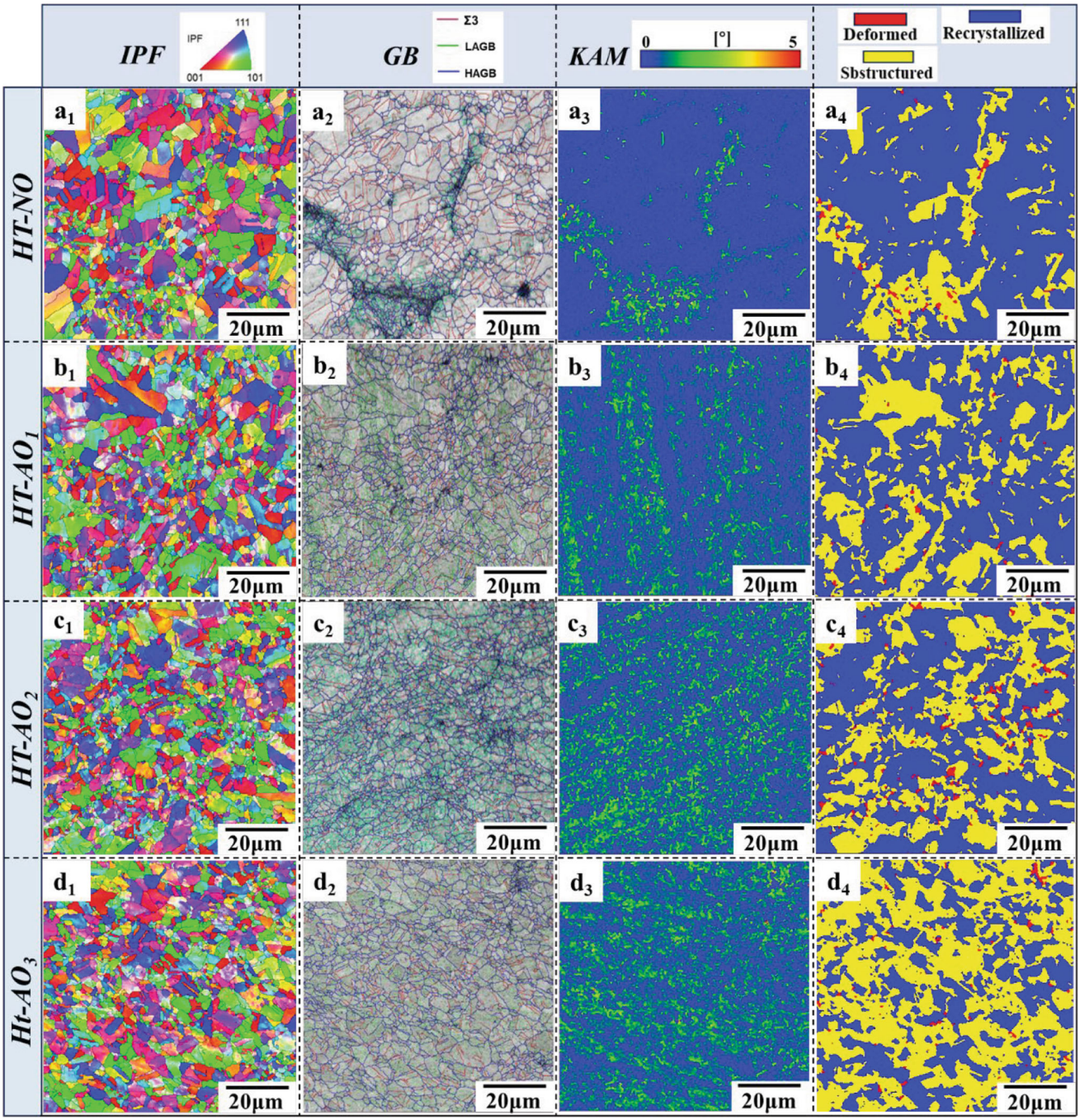

Fig. 11 EBSD data of post-spray heat-treated Ni coatings with different oxygen-content powders: (a_1-d_1) IPF maps, (a_2-d_2) GB maps, (a_3-d_3) KAM maps, and (a_4-d_4) recrystallization fraction. (a_1-a_4) HT-NO, (b_1-b_4) HT-OA_1, (c_1-c_4) HT-AO_2, and (d_1-d_4) HT-AO_3

between particles within the coating, reduces the number of defects and transitions the coating from brittle fracture to ductile fracture. The tensile fracture surface of the HT-NO (Fig. 14a_1, a_2) shows noticeable dimples and cracks propagate through the particles (shown in the yellow arrows of Fig. 14a_2). The tensile strength of the heat-treated coatings

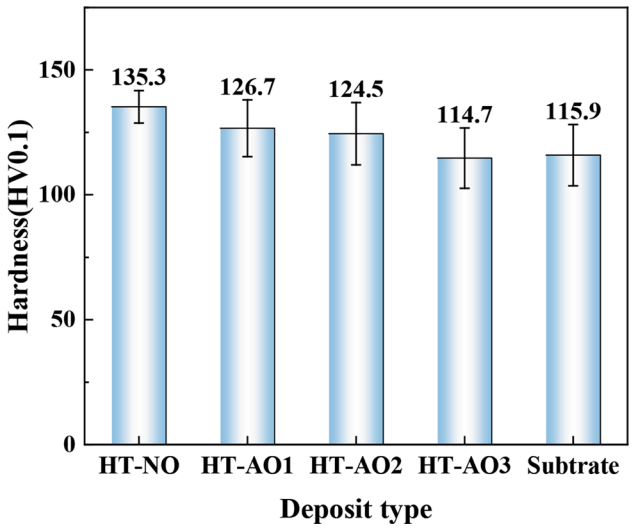

Fig. 12 Microhardness of post-spray heat-treated Ni coatings using different oxidized powders and Ni substrate

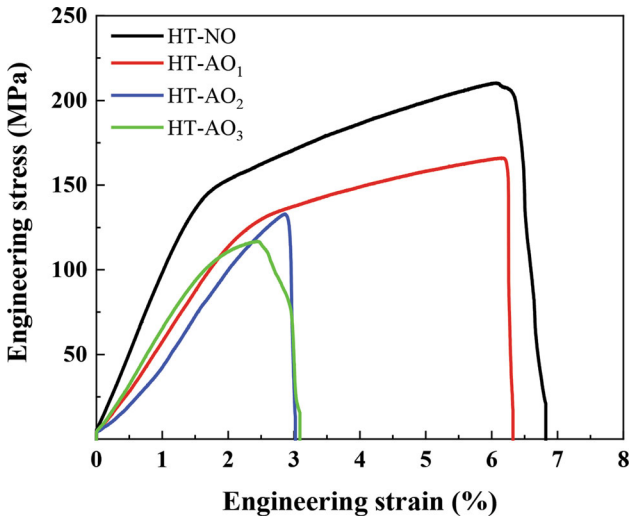

Fig. 13 Tensile stress vs. strain curves of post-spray heat-treated Ni coatings produced with different oxidized powders

using AO_1, AO_2 and AO_3 as feedstock powders reaches 166, 133 and 117 MPa, respectively, with corresponding strain values of 6.3, 3.0 and 3.1%. Noticeably, for the tensile fracture surface of the HT-AO_2(Fig. 14c_1, c_2) and the HT-AO_3 (Fig. 14d_1, d_2), the cracks propagate along the interface between particles, with a smooth fracture surface and prominent cleavage platform, so still exhibit characteristics of brittle fracture. The thicker oxide film on the surfaces of particles significantly weakens the inter-particle bonding capability within the coating, with the predominant form of particle–particle bonding remaining mechanical bounding. As a result, the strength and plasticity of the coating are challenging to enhance.

Conclusions

For the cold spray of Ni, this study investigated the correlation between the oxygen contents of feedstock powders and the properties of Ni coatings, and the following conclusions could be drawn:

(1) When the feedstock oxygen contents are 0.21 (NO), 0.27 (AO_1), 0.36 (AO_2) and 0.41 wt.% (AO_3), the corresponding porosities in as-sprayed Ni coatings are 0.4, 0.7, 1.5 and 3.3%, respectively. As the oxygen content of feedstock increases, the increase in the residual oxide film results in the coating in more nonbonded interfaces between the deposited particles, which reduces the coating density.

(2) The increase of oxide film thickness reduced the plastic deformation of impact particles and weakened the work-hardening effect of deformed particles, thus decreasing the microhardness of as-sprayed Ni coatings. The microhardness values of coatings produced with the feedstock oxygen contents of 0.21 (NO), 0.27 (AO_1), 0.36 (AO_2) and 0.41 wt.% (AO_3) were 289.2 $HV_{0.1}$, 263.2 $HV_{0.1}$, 245.3 $HV_{0.1}$ and 236.3 $HV_{0.1}$, respectively.

(3) The presence of a large number of defects and nonbonded interfaces in the as-sprayed Ni coatings resulted in a decrease in tensile strength. The tensile strength of the coatings produced with different feedstock oxygen content powders of 0.21 (NO), 0.27 (AO_1), 0.36 (AO_2) and 0.41 wt.% (AO_3) were 208, 94, 76 and 61 MPa, respectively.

(4) After heat treatment at 800 °C for 2 h, the number of defects and nonbonded interfaces in heat-treated Ni coatings was significantly reduced. After post-heat treatment, deformed grains were replaced by equiaxed grains and annealing twins, which increased the grain size, reduced the overall dislocation density and eliminated the residual stresses caused by the work hardening for as-sprayed coatings. However, as the oxide film content of the impact particles increased, the increase in atomic diffusion resistance weakened the healing capability of nonbonded interfaces during heat treatment.

(5) The strength and plasticity of heat-treated Ni coatings were improved, while the microhardness decreased significantly. The tensile strengths of heat-treated Ni coatings with feedstock oxygen contents of 0.21 wt.% (NO), 0.27 wt.% (AO_1), 0.36 wt.% (AO_2) and 0.41 wt.% (AO_3) were 210, 166, 133 and 117 MPa, respectively. The microhardness values of heat-treated Ni coatings were 135.3 $HV_{0.1}$, 126.7 $HV_{0.1}$, 124.5 $HV_{0.1}$ and 114.7 $HV_{0.1}$, respectively.

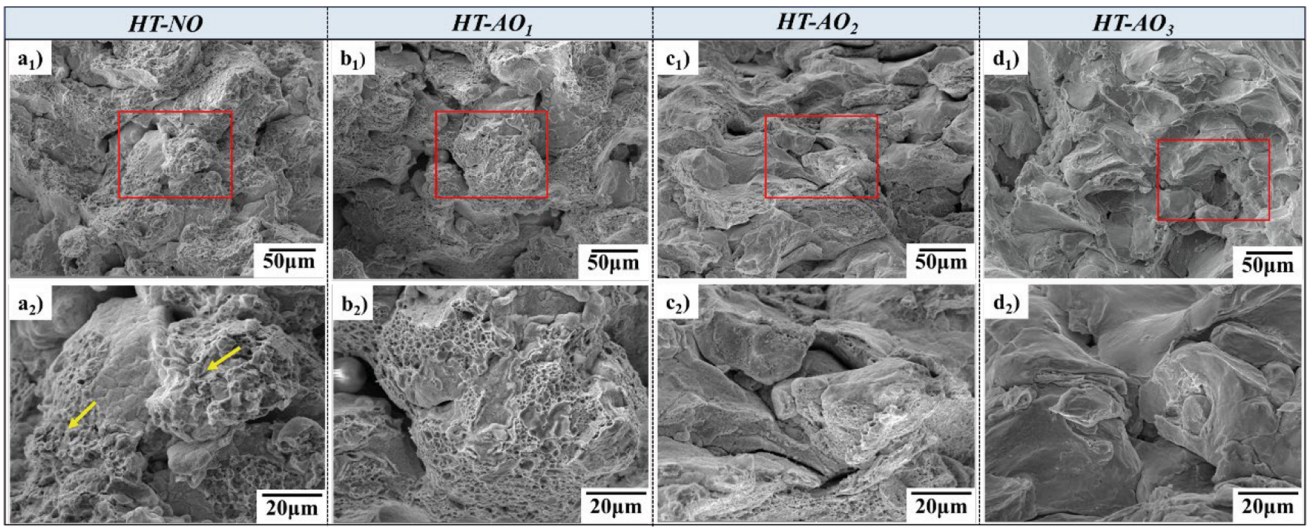

Fig. 14 SEM fractographic images of post-spray heat-treated Ni coatings with different oxidized powders: (a_1-a_2) HT-NO, (b_1-b_2) HT-AO_1, (c_1-c_2) HT-AO_2, (d_1-d_2) HT-AO_3. (a_2-d_2) respective enlarged views of the red boxes in (a_1-d_1). The yellow arrows represent the internal fracture cracks of particles (Color figure online)

Acknowledgments This work was supported by the National Natural Science Foundation of China (No.52061135101), the German Research Foundation (DFG,448318292), the Technology Innovation Guidance Special Foundation of Shaanxi Province (2023GXLH-085) and the Project of Key areas of innovation team in Shaanxi Province (2024RS-CXTD-20).

References

1. C.J. Huang, A. List, L. Wiehler, M. Schulze, F. Gärtner and T. Klassen, Cold Spray Deposition of Graded Al-SiC Composites, *Addit. Manuf.*, 2022, **59**, p 103116.
2. S. Yin, X.K. Suo, Y.C. Xie, W.Y. Li, R. Lupoi and H.L. Liao, Effect of Substrate Temperature on Interfacial Bonding for Cold Spray of Ni onto Cu, *J. Mater. Sci.*, 2015, **50**(22), p 7448–7457.
3. M. Yu, W.Y. Li, F.F. Wang, X.K. Suo and H.L. Liao, Effect of Particle and Substrate Preheating on Particle Deformation Behavior in Cold Spraying, *Surf. Coat. Technol.*, 2013, **220**, p 174–178.
4. W.Y. Li, C.C. Cao and S. Yin, Solid-State Cold Spraying of Ti and Its Alloys: A Literature Review, *Prog. Mater. Sci.*, 2020, **110**, p 100633.
5. W.Y. Li, X.P. Guo, C. Verdy, L. Dembinski, H.L. Liao and C. Coddet, Improvement of Microstructure and Property of Cold-Sprayed Cu-4 at.%Cr-2 at.%Nb Alloy by Heat Treatment, *Scr. Mater.*, 2006, **55**(4), p 327–330.
6. C.J. Huang, A. List, J.J. Shen, B.L. Fu, S. Yin, T. Chen, B. Klusemann, F. Gärtner and T. Klassen, Tailoring Powder Strengths for Enhanced Quality of Cold Sprayed Al6061 Deposits, *Mater. Des.*, 2022, **215**, p 110494.
7. J.C. Miranda and A. Ramalho, Abrasion Resistance of Thermal Sprayed Composite Coatings with a Nickel Alloy Matrix and a WC Hard Phase. Effect of Deposition Technique and Re-Melting, *Tribol. Lett.*, 2001, **11**(1), p 37–48.
8. J.K. Xiao, Y.Q. Wu, W. Zhang, J. Chen, X.L. Wei and C. Zhang, Microstructure, Wear and Corrosion Behaviors of Plasma Sprayed NiCrBSi-Zr Coating, *Surf. Coat. Technol.*, 2019, **360**, p 172–180.
9. X.S. Wang, Z.G. Xing, Y.P. Liu, J.J. Hou and K. Liu, Composite Ceramic-Ni60 Coating Fabricated via Supersonic Plasma Spraying, *Chin. J. Phys.*, 2019, **61**, p 72–79.
10. L. Ajdelsztajn, B. Jodoin and J.M. Schoenung, Synthesis and Mechanical Properties of Nanocrystalline Ni Coatings Produced by Cold Gas Dynamic Spraying, *Surf. Coat. Technol.*, 2006, **201**(3–4), p 1166–1172.
11. Z.M. Zhang, Y.X. Xu, W.Y. Li, J.W. Yang and C.J. Huang, Effect of Powder Particle Size on Microstructure and Mechanical Properties of Cold-Sprayed Pure Nickel Coatings, *J. Therm. Spray Technol.*, 2024, **33**, p 341–350.
12. Y. Zou, W. Qin, E. Irissou, J.G. Legoux, S. Yue and J.A. Szpunar, Dynamic Recrystallization in the Particle/Particle Interfacial Region of Cold-Sprayed Nickel Coating: Electron Backscatter Diffraction Characterization, *Scr. Mater.*, 2009, **61**(9), p 899–902.
13. G. Bae, K. Kang, H. Na, J.J. Kim and C. Lee, Effect of Particle Size on the Microstructure and Properties of Kinetic Sprayed Nickel Coatings, *Surf. Coat. Technol.*, 2010, **204**(20), p 3326–3335.
14. K. Kang, S. Yoon, Y. Ji and C. Lee, Oxidation Dependency of Critical Velocity for Aluminum Feedstock Deposition in Kinetic Spraying Process, *Mater. Sci. Eng. A Struct. Mater. Prop. Microstruct. Process.*, 2008, **486**(1–2), p 300–307.
15. S. Yin, X.F. Wang, W.Y. Li, H.L. Liao and H.E. Jie, Deformation Behavior of the Oxide Film on the Surface of Cold Sprayed Powder Particle, *Appl. Surf. Sci.*, 2012, **259**, p 294–300.
16. W.Y. Li and W. Gao, Some Aspects on 3D Numerical Modeling of High Velocity Impact of Particles in Cold Spraying by Explicit Finite Element Analysis, *Appl. Surf. Sci.*, 2009, **255**(18), p 7878–7892.
17. W.Y. Li, C.J. Li and H.L. Liao, Significant Influence of Particle Surface Oxidation on Deposition Efficiency, Interface Microstructure and Adhesive Strength of Cold-Sprayed Copper Coatings, *Appl. Surf. Sci.*, 2010, **256**(16), p 4953–4958.
18. C.Y. Chen, Y.C. Xie, R.Z. Huang, S.H. Deng, Z.M. Ren and H.L. Liao, On the Role of Oxide Film's Cleaning Effect Into the Metallurgical Bonding during Cold Spray, *Mater. Lett.*, 2018, **210**, p 199–202.
19. W.Y. Li, C. Zhang, H.T. Wang, X.P. Guo, H.L. Liao, C.J. Li and C. Coddet, Significant Influences of Metal Reactivity and Oxide

Films at Particle Surfaces on Coating Microstructure in Cold Spraying, *Appl. Surf. Sci.*, 2007, **253**(7), p 3557–3562.
20. H. Assadi, H. Kreye, F. Gärtner and T. Klassen, Cold Spraying—A Materials Perspective, *Acta Mater.*, 2016, **116**, p 382–407.
21. C.J. Li, W.Y. Li and H.L. Liao, Examination of the Critical Velocity for Deposition of Particles in Cold Spraying, *J. Therm. Spray Technol.*, 2006, **15**(2), p 212–222.
22. K. Kim, W.Y. Li and X.P. Guo, Detection of Oxygen at the Interface and Its Effect on Strain, Stress, and Temperature at the Interface Between Cold Sprayed Aluminum and Steel Substrate, *Appl. Surf. Sci.*, 2015, **357**, p 1720–1726.
23. W.Y. Li, H.L. Liao, C.J. Li, H.S. Bang and C. Coddet, Numerical Simulation of Deformation Behavior of Al Particles Impacting on Al Substrate and Effect of Surface Oxide Films on Interfacial Bonding in Cold Spraying, *Appl. Surf. Sci.*, 2007, **253**(11), p 5084–5091.
24. S. Rahmati, R.G.A. Veiga, A. Zúñiga and B. Jodoin, A Numerical Approach to Study the Oxide Layer Effect on Adhesion in Cold Spray, *J. Therm. Spray Technol.*, 2021, **30**(7), p 1777–1791.
25. Y. Ichikawa, R. Tokoro, M. Tanno and K. Ogawa, Elucidation of Cold-Spray Deposition Mechanism by Auger Electron Spectroscopic Evaluation of Bonding Interface Oxide Film, *Acta Mater.*, 2019, **164**, p 39–49.
26. C.J. Huang, M. Arseenko, L. Zhao, Y.C. Xie, A. Elsenberg, W.Y. Li, F. Gärtner, A. Simar and T. Klassen, Property Prediction and Crack Growth Behavior in Cold Sprayed Cu Deposits, *Mater. Des.*, 2021, **206**, p 109826.
27. H. Jazaeri and F.J. Humphreys, The Transition from Discontinuous to Continuous Recrystallization in Some Aluminium Alloys I—The Deformed State, *Acta Mater.*, 2004, **52**(11), p 3239–3250.
28. Y. Zou, A. Rezaeian, J.A. Szpunar, E. Irissou and S. Yue, Structural Transformation and Mechanical Properties of Cold Sprayed Nickel Coatings after Annealing, *MRS Online Proc. Libr.*, 2008, **1151**(1), p 61–66.
29. H. Koivuluoto and P. Vuoristo, Structural Analysis of Cold-Sprayed Nickel-Based Metallic and Metallic-Ceramic Coatings, *J. Therm. Spray Technol.*, 2010, **19**(5), p 975–989.
30. C. Huang, T. Chen, B. Fu, Z. Zhang, A. List, B. Klusemann, W. Li, F. Gaertner, and T. Klassen, Ductility and Fracture Behavior of Cold Spray Additive Manufactured Zinc. *Addit. Manuf.*, 2024, **89**, p 104310.
31. W. Li, J. Yang, Z. Zhang, Y. Xie, and C. Huang, High Ductility Induced by Twin-Assisted Grain Rotation and Merging in Solid-State Cold Spray Additive Manufactured Cu. *J. Mater. Sci. Technol.*, 2024. https://doi.org/10.1016/j.jmst.2024.06.032